REVISTA MATÉRIA V.30
ISSN 1517-7076 articles e20250164, 2025

Enhancing concrete performance with geogrid confinement and fiber reinforcement: an experimental study

Selvapriya Velusamy[1], Ramadevi Kanagaraj[2], Divyah Nagarajan[1]

[1]PSG Institute of Technology and Applied Research, Department of Civil Engineering. Tamil Nadu, India.
[2]Kumaraguru College of Technology, Department of Civil Engineering. Tamil Nadu, India.
e-mail: vsp@psgitech.ac.in, ramadevi.k.ce@kct.ac.in, divyah@psgitech.ac.in

ABSTRACT

This study investigates the impact of internal geogrid confinement combined with fiber reinforcement on the axial behavior of concrete stub columns. Twenty small-scale circular stub column specimens were prepared, incorporating variations in the number of geogrid layers (one, two, and three) and fiber types (steel and polyvinyl alcohol). Results showed that geogrid confinement enhanced the axial load capacity, with double and triple layers improving the load by 10% and 8%, respectively, compared to unconfined specimens. Incorporating fibers further elevated performance, with PVA fibers yielding higher axial strength than steel fibers. Samples reinforced with geogrid and steel fibers exhibited superior fracture energy absorption, particularly in specimens with triple geogrid layers. Both geogrid and fiber-reinforced specimens demonstrated markedly improved load-deformation behavior and higher ductility indices. While geogrid confinement did not substantially increase the ultimate load capacity, it significantly enhanced ductility and energy absorption, suggesting that geogrids present a promising alternative to conventional confinement methods. Future work should focus on comparing uniaxial and biaxial geogrid effects and assessing performance under aggressive environmental conditions.

Keywords: Geogrid; Confinement; Stub Column; Fiber Reinforcement; Ductility.

1. INTRODUCTION

Stub columns are essential structural elements that transfer loads from beams and slabs to foundations, particularly in designs requiring efficient use of limited space. Their stability is critical to the overall integrity of buildings, making them highly susceptible to failure under dynamic stresses, such as seismic events or impact loads. Ensuring the ductile behavior of these columns is therefore vital for enhancing the safety and resilience of reinforced concrete (RC) structures. Many research investigations examined the stub columns from a variety of angles to improve their adaptability for unique applications [1, 2]. One of the structural components most susceptible to collapse under fluctuating stress and impact stress from earth tremors or shock loads is reinforced concrete columns. When columns fail, the structure they support frequently collapses catastrophically. Therefore, it is essential to ensure the ductile behavior of vertical elements in reinforced concrete (RC) buildings. Consequently, an enormous amount of study has been done to assess the way various fiber forms and stirrup configurations affect the bending and shear capacity of RC elements. This study deals with the utilization of geogrids, which are geosynthetic materials that are gaining familiarity in the infrastructure sector of the construction industry. Various research studies have shown the great potential and important advantages of implementing geogrids for a range of innovative construction applications [3–5]. On the other hand, not much research has been done on the use of geogrids in place of rebar in columns. In order to increase stability and reduce lateral deformation, geogrid is introduced as a tensile component, which is inserted inside the concrete column's periphery in stub columns. Before the concrete stub column is cast, geogrids are placed into the mould. The geogrids' tensile strength can be put to beneficial use because it could be shaped into a circle without having any sharp bends. The interior layer of geogrid behaved similarly to the traditional transverse reinforcement [6]. They are more ductile in nature so that they provide tensile resistance when the loaded columns expand and prevent cracks from propagating through their ribs. Furthermore, the provision of internal confining geogrids with excellent durability and zero susceptibility to corrosion provides a possibility in the potential trimming of the thickness of the cover concrete.

Corresponding Author: Selvapriya Velusamy Received on 20/02/2025 Accepted on 26/06/2025

DOI: https://doi.org/10.1590/1517-7076-RMAT-2025-0164

The geogrid is a geosynthetic material that features a grid pattern and various opening sizes. Extruded polypropylene or woven textiles make up the most popular types of geogrids. The comprising materials, mechanical qualities, and physical attributes that vary depending upon the particular requirements of the application. Based on the directions of the rib extension, one can categorize geogrids as uniaxial, biaxial, or triaxial. Lateral confinement is achieved while the geogrid's aperture size is equal to the aggregate particle size.

Extensive research has explored various means of improving the ductility and load-carrying capacity of RC columns, including the use of different fiber types and stirrup configurations. However, the use of geogrids synthetic materials commonly employed in soil stabilization and pavement reinforcement as internal confinement elements in concrete columns remains relatively underexplored. Very little research has been published related to the application of geosynthetics as a confining material in concrete columns. Additionally, geogrid-confined columns are not covered by structural design regulations, specifications, or standards. Despite the promising structural benefits demonstrated through experimental investigations, the application of geogrid confinement in concrete elements remains largely absent from major international design standards. Notably, design guidelines such as ACI 440 (U.S.) and CEB-FIB Model Code (Europe) primarily focus on the use of fiber-reinforced polymers (FRP) for external confinement and do not provide specifications or design provisions for internal confinement using geosynthetics like geogrids. This gap limits the widespread adoption of geogrids in structural concrete applications. The absence of codified design models hinders accurate prediction of performance parameters such as strength, ductility, and long-term durability. Furthermore, most available models are based on FRP-confined behavior, which differs in material properties and confinement mechanics from geogrids. To incorporate geogrid confinement into structural design practice, further experimental validation, analytical modeling, and development of reliable stress-strain models are essential. Only through rigorous standardization and code inclusion can the use of geogrids be confidently adopted in real-world structural engineering applications. On the other hand, several well-controlled experimental, analytical, and numerical research projects are required to close this gap. Geogrids are more advantageous than other materials since they are corrosion resistant, lightweight, inexpensive, readily available for commercial use, simple to manufacture, and sustainable. In structural application, each of these characteristics is important.

Concrete structural elements, particularly columns, are prone to failure under dynamic and high-intensity loads. Various studies have explored methods to enhance the ductility and strength of such elements, especially through innovative reinforcement strategies. Among these, the incorporation of geogrid materials has gained considerable attention. Geogrids, known for their corrosion resistance, light weight, and sustainability, have been evaluated for their potential as an alternative to conventional transverse reinforcement. Numerous studies have underscored the capacity of geogrid confinement to improve the mechanical performance of concrete elements. AL-AYASH *et al*. [7] demonstrated that plain cement concrete cylinders confined with uniaxial and biaxial geogrids exhibited enhanced ductility, particularly after initial cracking, compared to unreinforced specimens. Their findings highlighted the advantage of biaxial geogrids in achieving higher ultimate axial stress, despite their relatively lower tensile strength compared to uniaxial geogrids. Similarly, EL MESKI and CHEHAB [8] observed that geogrid-reinforced concrete beams, whether conventional or high-strength, exhibited greater ductility and deflection under monotonic loading than unreinforced beams, although initial cracking occurred earlier due to the weaker sections introduced by the geogrid layers.

TANG *et al*. [9] further extended this understanding by comparing rigid and flexible biaxial geogrids in concrete members, revealing that rigid geogrids significantly improved energy absorption and post-cracking ductility, particularly when two layers were used. This reinforces the importance of geogrid material properties in determining reinforcement effectiveness. In a related study, SIVAKAMASUNDARI *et al*. [10] evaluated the combined effect of steel fibers and biaxial geogrids in both tension and compression, concluding that the inclusion of steel fibers amplified the energy dissipation capacity and post-cracking behavior of geogrid-reinforced concrete. Other investigations have looked into the secondary benefits of geogrid reinforcement. AL-HEDAD *et al*. [11] explored the impact on drying shrinkage in concrete pavements and found that geogrid layers could reduce shrinkage strains by up to 28%, with placement closer to the surface yielding better results. These findings reveal that the influence of geogrids extends beyond strength and ductility, impacting dimensional stability as well.

In terms of hybrid reinforcement systems, SIVA CHIDAMBARAM and AGARWAL [12] confirmed that combining steel fibers with geogrid confinement enhances load-displacement behavior under both compression and flexure. Subsequent studies by SIVA CHIDAMBARAM and AGARWAL [13, 14] expanded on this by evaluating beam-column joints and RC beams, showing that such combinations can alter failure modes and significantly improve energy dissipation and ductile performance under cyclic loading. Their research further indicates that geogrid confinement, particularly when paired with steel fibers, enhances post-cracking response and crack control.

SIVA CHIDAMBARAM and AGARWAL [15], investigated the shear behavior under static and cyclic loads using geogrid confinement material in reinforced concrete elements. Six different R/C beam types were evaluated, along with four beam-column specimens that had geogrid confinement and a modified stirrups ratio. Examining the impact of confinement provided by geogrid on the shear capacity at various transverse reinforcement spacings was the primary goal of the study. It was expected that the shear resistance and post-cracking response of reinforced concrete beam elements would be improved by the composite action of geogrid and steel fibers with larger stirrup spacing. The load deformation plot, strength as well as stiffness deterioration, facture energy, and patterns of failure were used to assess the behaviour of tested specimens. It was found that adding geogrid to the RC elements increased the resistance against shear and enhanced the inelastic response. The combined action provided by the geogrid and the lowest possible quantity of steel fibers in the RC beam elements improved the energy absorption and also provided improved crack propagation.

However, the performance of geogrids under adverse conditions remains a topic of scrutiny. YALCINER *et al*. [16] studied RC beams under induced corrosion and concluded that geogrid confinement, though beneficial in non-corrosive environments, underperformed compared to conventional reinforcement when corrosion was introduced. This underlines the contextual limitations of geogrid applications.

Fiber-reinforced polymer (FRP) was employed in columns made with concrete by MANDER *et al*. [17]. It was concluded that the load-resisting capacity and ductility of concrete may be greatly enhanced by providing confinement with FRP externally. Encasing the concrete column using FRP laminates is one way to confine it. The layers are parallel to the direction of hoop stress and fastened to the outer surface of the column. Numerous exploratory investigations have been carried out in this field; they include those investigated by HADI [18], LAM and TENG [19], LI and HADI [20], and FAM and RIZKALLA [21].

LAM and TENG [19] also support the general notion that confinement improves ductility and strength, with analytical models showing that significant post-peak strength enhancement is attainable when confinement ratios exceed a certain threshold. Recent investigations by VELAYUTHAM *et al*. [22] explored the structural performance of GFRP-concrete-steel composite columns under eccentric axial loading. Their study demonstrated that GFRP sections can significantly enhance ductility and energy dissipation capacity, highlighting their viability in hybrid composite configurations where corrosion resistance and structural integrity are critical.

SALMAN and ALLAWI [23] conducted an experimental and numerical study on the behavior of reinforced concrete composite columns encased with GFRP and steel I-sections under concentric, eccentric, and flexural loading conditions. The investigation included twenty-one specimens of varying heights and load types to examine the impact of confinement using I-sections. Their findings revealed that hybrid GFRP-steel encased columns exhibited comparable failure modes and load-deformation characteristics to those with only steel I-sections. Notably, GFRP encasement improved ductility and strength, particularly in slender and short columns. The study also developed interaction diagrams (N-M) using finite element modeling through ABAQUS, validating them with experimental data. These results support the potential of using GFRP as an alternative to steel for internal confinement, aligning with the present investigation's focus on innovative, corrosion-resistant confinement methods like geogrids.

AHMED *et al*. [24] carried out a thorough experimental study on composite circular reinforced concrete columns encased with pultruded glass fiber reinforced polymer (GFRP) and steel I-sections to examine their behavior under concentric, eccentric, and flexural loading conditions. Their research showed that GFRP and steel encasements both improved the ultimate load-carrying capacity and ductility of concrete columns over unconfined specimens. Though steel I-sections showed greater increases in strength, GFRP I-sections showed significant improvement, with a gain of up to 9.7% in eccentric loading and 36.6% in flexural loading. The authors further noted that columns encased with GFRP showed more ductile failure patterns and improved post-peak behavior compared to control specimens, which indicates the viability of using GFRP profiles as a substitute for traditional steel for internal confinement. This paper highlights the significance of researching other confinement materials such as GFRP for use in structural applications, particularly enhancing seismic resistance and minimizing corrosion-induced deterioration.

ALLAWI *et al*. [25] conducted a sophisticated finite element analysis with ABAQUS to model the behavior of glass fiber reinforced polymer (GFRP) I-section fully encased concrete composite circular columns under concentric, eccentric (25 mm and 50 mm), and flexural load. Their models were verified with experiments, exhibiting highly consistent agreement with respect to ultimate strength, failure modes, and deformation behavior. The findings showed that both steel I-sections and GFRP enormously improved column performance in different loading modes, with GFRP-confined specimens showing up to 7.6% and 31% improved strength in eccentric and flexural conditions, respectively, compared with unconfined counterparts. The research also created axial load–bending moment interaction diagrams, which show that GFRP encasement is a structural

equivalent of steel with the advantages of corrosion resistance and reduced weight. This quantitative research is favorable for the possible use of GFRP profiles in hybrid confinement systems, rendering it pertinent for assessing other confinement options like geogrid application in reinforced columns. In addition, SALMAN and ALLAWI [26] investigated the strength and deformation behavior of reinforced concrete columns encased with both I-section steel and I-section GFRP profiles under concentric, eccentric, and lateral loading. Their experimental results demonstrated that while steel-encased columns achieved higher overall strength, GFRP-encased columns offered significant improvements in ductility and energy absorption. The GFRP-confined specimens showed more stable post-peak behavior, suggesting their suitability for applications where controlled failure and seismic resilience are desired. This study contributes valuable comparative insight into the behavior of alternative confinement materials and supports the adoption of corrosion-resistant GFRP profiles for structural applications. The findings directly align with the current investigation's focus on geogrid-based confinement as a viable substitute for traditional reinforcement methods.

RAVIKUMAR *et al*. [27] examined the crushing performance of pultruded GFRP angle sections under various joint configurations in lattice towers. Their results emphasized the effectiveness of hybrid bolted-adhesive joints in resisting axial loads, which could be conceptually aligned with confinement mechanisms in composite columns. Similarly, ASSUNÇÃO *et al*. [28] investigated the mechanical performance of glass fiber-reinforced polyester composites fabricated using different spray-up methods, showing notable improvements in impact resistance and reliability when produced with vacuum-assisted molding. These findings help contextualize the mechanical behavior of GFRP-based confinement systems and support the exploration of alternative composite techniques in structural elements. In related research, SHAHRBIJARI *et al*. [29] examined the performance of concrete beams reinforced with pre-stressed Glass Fiber Reinforced Polymer (GFRP) and conventional steel bars. Their experimental program evaluated key structural parameters including deflection, crack width, stiffness, and failure modes. The findings showed that beams reinforced with pre-stressed GFRP exhibited comparable load-carrying capacity and improved serviceability compared to their steel-reinforced counterparts, with significant reductions in crack widths and enhanced flexural performance. Moreover, GFRP-reinforced beams demonstrated a more favorable post-yield behavior and ductility when appropriately pre-stressed. These results underscore the viability of GFRP as a primary reinforcement material in structural concrete members and lend support to current investigations involving GFRP alternatives such as geogrid confinement in enhancing mechanical behavior.

From the above analysis, it is evident that while the type, orientation, and number of geogrid layers influence mechanical performance, combining geogrids with fibers especially steel consistently yields better ductility, energy absorption, and post-cracking performance. Despite these promising outcomes, the use of geogrids in structural applications remains under-represented in design codes, and their behavior under long-term environmental exposure warrants further investigation.

This study aims to bridge that gap by experimentally evaluating the performance of stub concrete columns confined internally with uniaxial geogrids and reinforced with steel and PVA fibers. The findings contribute to a more refined understanding of how geogrid confinement can be effectively utilized in structural concrete elements to enhance performance without significantly altering the ultimate load-bearing capacity. Table 1 provides list of symbols, notations and abbreviations used in this article.

2. SPECIMEN AND TEST PARAMETERS

Twenty small-scale stub column specimens having a diameter of 150 mm and a depth of 300 mm were exposed to an axial compressive load. The primary test variables were the number of geo-grid layers and fiber material. Based on the confining material layer and fiber type, four series (UC, C-E, CS-E, and CP-E) were adopted in the categorization of the specimens. The term UC denotes the stub column specimen without confinement and without fiber, the term C-E represents stub columns confined with uniaxial geogrids, whereas the term CS-E represents steel fiber reinforced stub columns confined with uniaxial geogrids, and the term CP-E represents PVA fiber reinforced stub columns confined with uniaxial geogrids. Table 2 provides specimen labels, sizes, and corresponding specifications for the test for all the specimens. 1L implies a single geogrid layer, 2L implies double layers of geogrid, and 3L implies three layers of geogrid.

2.1. Testing and materials

In the present experiment, concrete mix in the proportion of cement: sand: aggregate as 1:1.4:3 using 43 grade Ordinary Portland Cement (OPC) according to the Indian standard [30]. Locally available manufactured sand (m – sand) of sieve size smaller than 4.75 mm is used as fine aggregate and broken aggregate of size smaller than 10 mm is adopted as coarse aggregate. The selected ratio of water to cement is 0.5. The target

Table 1: The list of symbols, notations and abbreviations used in this paper.

SYMBOL/ABBREVIATION	DEFINITION
OPC	Ordinary Portland Cement
RC	Reinforced Concrete
FRP	Fiber Reinforced Polymer
UTM	Universal Testing Machine
MD	Machine Direction (of geogrid)
CMD	Cross Machine Direction (of geogrid)
PVA	Polyvinyl Alcohol
GFRP	Glass Fiber Reinforced Polymer
CEB-FIP	Comité Euro-International du Béton – Fédération Internationale de la Précontrainte
ACI	American Concrete Institute
UC	Unconfined Control Specimen (no geogrid or fiber)
C-E	Specimens Confined with Geogrid Only
CS-E	Specimens Confined with Geogrid and Steel Fibers
CP-E	Specimens Confined with Geogrid and PVA Fibers
1L, 2L, 3L	Number of Geogrid Layers: One, Two, or Three
f'_c	Compressive Strength of Concrete (MPa)
E_c	Modulus of Elasticity of Concrete (GPa)
f_t	Tensile Strength of Concrete (MPa)
f_r	Modulus of Rupture (MPa)
A_c	Cross-sectional Area of Concrete (mm^2)
P_{max}	Maximum Axial Load Carried by Specimen (kN)
α	Ratio of Maximum Load of Specimen to Control Sample Load
δ_y	Axial Deformation at Yield Point (mm)
δ_f	Axial Deformation at 50% of Ultimate Load (mm)
μ	Displacement Ductility Index (δ_f/δ_y)
F	Fracture Energy (N-m)
K	Energy Ductility Index (Ratio of Fracture Energy to Control Specimen)

Table 2: Details of test samples.

SAMPLE ID	CONFINEMENT	TYPE OF FIBRE	NUMBER OF GEOGRID LAYERS
UC	None	None	–
C-E-1L	Geogrid-60 kN/m	None	1
C-E-2L	Geogrid-60 kN/m	None	2
C-E-3L	Geogrid-60 kN/m	None	3
CS-E-1L	Geogrid-60 kN/m	Steel	1
CS-E-2L	Geogrid-60 kN/m	Steel	2
CS-E-3L	Geogrid-60 kN/m	Steel	3
CP-E-1L	Geogrid-60 kN/m	PVA	1
CP-E-2L	Geogrid-60 kN/m	PVA	2
CP-E-3L	Geogrid-60 kN/m	PVA	3

strength of concrete mixture was 26.6 Mpa. Curing of all the beam specimens were done for 28 days. Standard cylindrical specimens having a depth of 300 mm and a diameter of 150 mm were casted as well as tested in order to determine the compressive strength of concrete. The concrete's average compressive strength at 28 days was 27 MPa. The estimated mechanical properties of the concrete mix, based on empirical expressions provided by IS 456:2000 [31] and ACI 318 [32], are summarized in Table 3 below.

Table 3: Estimated mechanical properties of the concrete.

PROPERTY	SYMBOL	VALUE	UNIT
Compressive strength	f'_c	27	MPa
Modulus of elasticity	E_c	25.96	GPa
Tensile strength	f_t	2.9	MPa
Modulus of rupture	f_r	3.2	MPa

2.2. Geogrids

The properties of geogrid material have a principal impact on the degree to which the mechanism of geogrid confinement works. The properties of the geogrids given by the manufacturer are listed in Table 4. The geogrids employed in this work are displayed in Figure 1. In all the single, two- and three-layered confined samples, the geogrid sheets were manually rolled and secured in place to achieve the required cylindrical shape.

By using a universal testing machine of 100 kN capacity, geogrid strands were tested in order to ascertain the properties of the material. The test was performed according to ASTM D-6637 [33]. According to method A prescribed in ASTM D6637, only one rib of geogrid is tested. The length the specimen adopted is 300 mm. The test framework for testing the geogrid is shown in Figure 2. Thirty millimeters per minute was the average speed at which the displacement-controlled test was conducted. Figure 3 displays the load-strain graph for the tested geogrid. In the setup illustrated in Figure 2, the geogrid specimen was clamped at both ends using specially designed serrated grips provided with the universal testing machine (UTM) to avoid slippage during the test. The top grip remained stationary, while the bottom grip was connected to the moving crosshead. These end restraints ensured a uniaxial tensile load was applied directly along the machine direction (MD) of the geogrid rib under test, in accordance with ASTM D6637 Method A. No additional supports or bearing plates were used, as the geogrid strip was treated as a single rib element isolated for axial loading. This ensured accurate measurement of load-elongation behavior while avoiding stress concentrations or eccentricities at the clamped ends.

2.3. Steel fiber

In this investigation, fresh concrete with a concrete volume percentage of 0.3% was combined with hook-end steel fibers. It is shown in Figure 4 that the steel fibers used in this investigation had a mean diameter of 0.30 mm and a length of 30 mm. It had a tensile strength of 1.95 GPa and a modulus of elasticity (Young's modulus) of 205 GPa. The volume fraction of steel fiber adopted for the present investigation is 0.3%.

Table 4: Properties of uniaxial geogrid.

DESCRIPTION	UNIT	VALUES
Load at a strain value of 2%	kN/m	8
Load at a strain value of 5%	kN/m	18
Ultimate Tensile Strength (MD*/CMD*)	kN/m	65/20
Size of the aperture (MD*/CMD*)	mm/mm	35/35
Breadth of the Rib (MD*/CMD*)	mm/mm	8/8
Thickness of the Rib (MD*/CMD*)	mm/mm	2/1
Thickness at Junction	mm	3

(MD* – Machine Direction/CMD* – Cross Machine Direction).

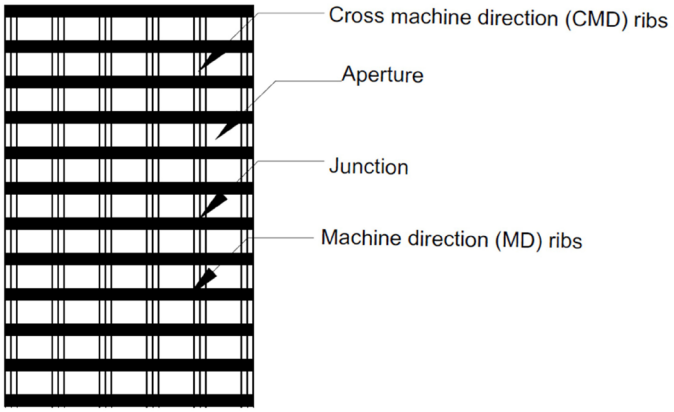

Figure 1: Diagrammatic representation of geo-grid in MD and CMD.

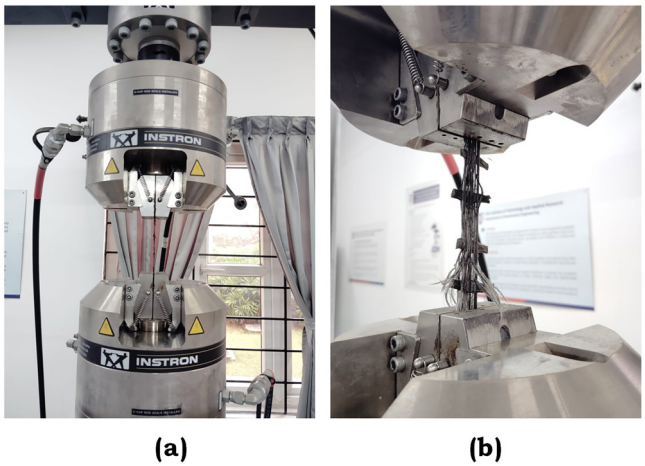

Figure 2: (a) Tension test setup for testing geogrid (b) geogrid placed between grips.

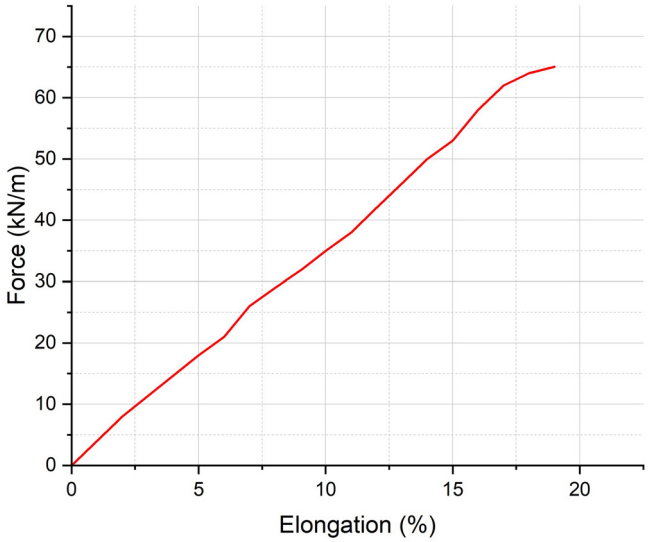

Figure 3: Force–elongation graph for the tested uni-axial geogrid material in machine direction.

Figure 4: Hooked end steel fiber used in the study.

Figure 5: PVA fiber used in the study.

2.4. Polyvinyl alcohol (PVA) fiber

PVA fiber provides advantageous qualities that increase the strength of concrete. Its tensile strength, bond strength, durability, and elasticity modulus are all high. These characteristics are necessary to increase the resilience of concrete. Being illustrated in Figure 5, the dimensions of PVA fiber are 38 μm in diameter, 8 mm in length, and 1.3 g/cm³. PVA fiber has a modulus elasticity that is higher than that of natural fiber, ranging from 25 to 40 GPa. The volume fraction of steel fiber adopted for the present investigation is 0.3%.

2.5. Sample preparation

A pan mixer was used to achieve the homogenous mix of the materials. Geogrid is formed into a cylindrical shape, as illustrated by Figure 6, and placed within the cylinder mold prior to the placement of concrete. Compaction was done by using a tamping rod to accomplish a target slump value of 100 mm. After demoulding, honeycombing was not visible in any of the specimens, and the specimens were kept in a curing tank.

2.6. Cross sectional details of samples

All specimens tested in this study had a circular cross-section with a diameter of 150 mm and a height of 300 mm, forming stub column elements. The uniaxial geogrid confinement was manually rolled into a cylindrical shape and inserted concentrically along the inner periphery of the mould before concrete casting, maintaining contact with the concrete to simulate confinement. No traditional steel bars or stirrups were included in the cross-section to isolate the confinement effect of geogrid and fiber. The concrete matrix was uniformly mixed with either steel or PVA fibers at a 0.3% volume fraction, ensuring an even fiber distribution across the

Figure 6: Geo-grid confined cylindrical specimen preparation.

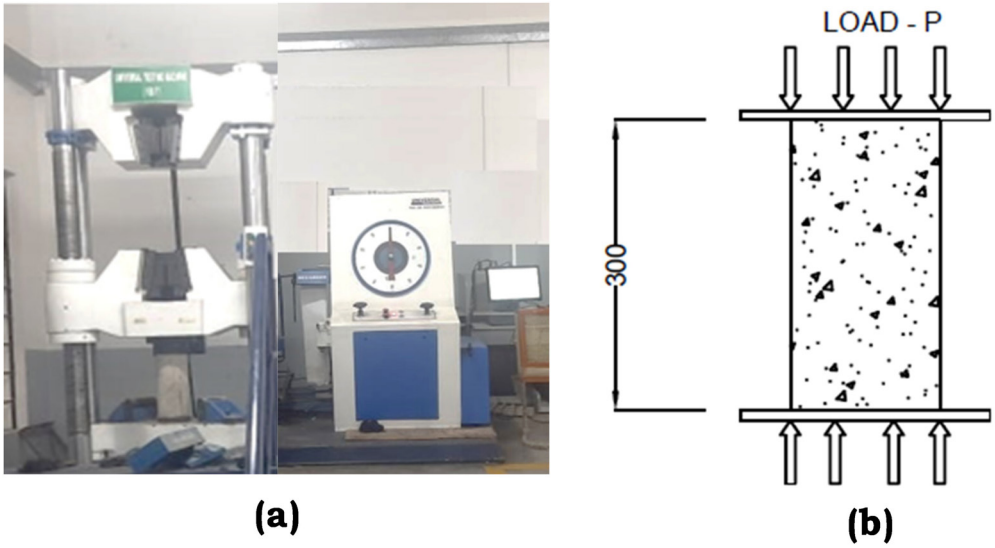

Figure 7: (a) Experimental setup for testing cylinders (b) load application method.

Note: All dimensions are in mm.

cross-section. There were no voids or hollows within the core. The geogrid layers overlap horizontally and were cut to match the circumference with minimal overlap at joints.

2.7. Testing and instrumentation

A computerized Universal testing machine (UTM) with a 1000 kN capacity has been used to perform the axial compression test. As illustrated in Figure 7a and 7b, cylindrical specimens have been positioned vertically to achieve the axial behaviour in compression. Applied load and related displacements were tracked and recorded by a data acquisition system, which is connected to the UTM.

3. RESULTS AND DISCUSSION

When the specimens were loaded, hairline longitudinal cracks appeared first on the outside of the specimens. These cracks then grew and spread throughout the central region, along with a series of high-pitched sounds made by geogrid connections breaking. At the final point of failure, the overlap took away the geogrid layer's

anchorage; most of the cover concrete had come apart, and the geogrid layer's ribs had broken. Every concrete specimen containing geogrid confinement revealed progressive failure. Failure occurred when there was an enormous outward expansion of the concrete core and a significant rupture of the geogrid.

The test findings are presented in Table 5, which incorporates the maximum axial compressive load applied (P_{max}) recorded, the ratio between the maximum load carried by the test sample and that of the unconfined sample (α), the axial displacements δ_f and δ_y, the ratio (μ) of axial displacements δ_f and δ_y, absorbed energy (F), and the ratio between the tested sample fracture energy and the control unconfined sample fracture energy (K). Referring to the load defmation graph in Figure 8 [6], P_y denotes the load at the yield point; it corresponds to the point where the load-deformation graph transforms as non-linear along with δ_y denoting the corresponding deformation. δ_f is the axial deformation that corresponding to 0.5 times the ultimate load reached [6].

In this investigation, two factors were utilized to assess the ductility related to the load-deformation behaviour. A structural component or element is said to be ductile if it can experience inelastic deformation without experiencing a significant reduction in resistance. The displacement ductility index, which is the axial deformation ratio (μ), is suggested as a first indicator for ductility related to the load-deformation behaviour. In this study, the region below the load-deformation graph up to δ_f(mentioned in the Figure 8) is referred to as fracture energy. Another indicator used for assessing the ductility related to the load-deformation behavior is K. It is the ratio (K) between the energy absorbed by the tested sample and that of the unconfined control sample. This is known by the Energy Ductility Index [6].

3.1. Analytical estimation of load capacity and experimental correlation

To provide a theoretical basis for the experimental results, a simplified calculation can be used to estimate the axial compressive strength of the geogrid-confined concrete columns. The nominal compressive strength (N) [32, 34] of a reinforced concrete column can be approximated by the following Equation 1.

$$N = A_c \cdot f_c + A_s \cdot f_s \tag{1}$$

where A_c is the cross-sectional area of the concrete, f_c is the nominal compressive strength of the concrete, A_s is the total area of the steel reinforcement (if applicable), f_s is the yield strength of the steel reinforcement. For the geogrid-confined columns in this study, the confinement effect of the geogrid can be analogously considered as an additional contribution to the compressive strength. The enhancement due to geogrid confinement can be empirically estimated based on the experimental results. Table 6 provides a preliminary theoretical estimate of the axial compressive strength. The calculation uses the simplified formula (since no steel rebars are mentioned

Table 5: Experimental results of the tested samples.

SAMPLE ID	MAXIMUM LOAD P_{max} (kN)	MAXIMUM LOAD RATIO α**	YIELD DEFLECTION δ_y*** (mm)	ULTIMATE DEFLECTION δ_f*** (mm)	DISPLACEMENT DUCTILITY INDEX μ+	FACTURE ENERGY (N-m)	ENERGY DUCTILITY INDEX K++
C	437	1	0.819	4.531	5.531	1416.55	1.000
C-E-1L	460.24	1.053	0.600	7.120	11.867	2382.04	1.682
C-E-2L	482.78	1.105	0.901	5.110	5.671	2277.33	1.608
C-E-3L	474.92	1.087	0.900	9.000	10.000	3567	2.518
CS-E-1L	438.16	1.003	1.122	10.230	9.118	3524.27	2.488
CS-E-2L	448.95	1.027	0.710	12.580	17.718	4235.14	2.990
CS-E-3L	444.92	1.018	0.870	12.610	14.494	4563.45	3.222
CP-E-1L	483.36	1.106	0.660	8.210	12.439	3061.21	2.161
CP-E-2L	474.2	1.085	0.670	8.440	12.597	3190.28	2.252
CP-E-3L	429.9	0.984	0.900	8.930	9.922	3003.39	2.120

**α denotes the ration between the maximum load of the tested sample P_{max} and the maximum load of the control sample C.

***δ_y and δ_f are described by Figure 8.

+μ is denoted by the ratio between δ_y and δ_f, which is also denoted as the displacement-ductility index.

++K is denoted by the ratio between energy absorbed by the tested sample and the energy absorbed by the control sample. Figure 8 defines the energy absorbed by the tested sample.

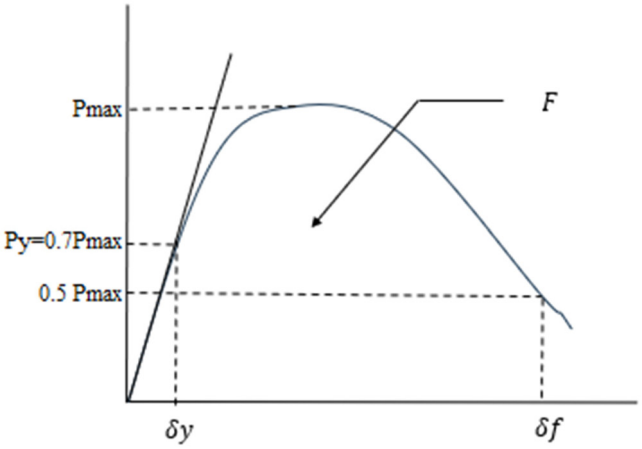

Figure 8: Diagram of a load-deformation graph to denote the variables utilized in Table 3.

Table 6: Analytical results.

SAMPLE ID	CONCRETE STRENGTH f_c (MPa)	CROSS-SECTIONAL AREA A_C (mm²)	BASE N (kN)	CONFINEMENT FACTOR (α)	ADJUSTED N (kN)	EXPERIMENTAL P_{max} (kN)
UC	27	17671	477.1	1.00	477.1	437.0
C-E-1L	27	17671	477.1	1.05	501.0	460.2
C-E-2L	27	17671	477.1	1.10	524.8	482.8
C-E-3L	27	17671	477.1	1.08	515.3	474.9
CS-E-1L	27	17671	477.1	1.003	478.5	438.2
CS-E-2L	27	17671	477.1	1.027	490.1	448.9
CS-E-3L	27	17671	477.1	1.018	485.9	444.9
CP-E-1L	27	17671	477.1	1.106	527.7	483.4
CP-E-2L	27	17671	477.1	1.085	517.7	474.2
CP-E-3L	27	17671	477.1	0.984	469.5	429.9

in the study) and includes an empirical adjustment for geogrid/fiber confinement based on the experimental results. The confinement factor (α) accounts for geogrid/fiber effects, derived from experimental load ratios (Table 3). This approach aligns with established confinement models suggested by MANDER *et al*. [17] and prior geogrid studies by DAOU *et al*. [6].

It is acknowledged that the theoretical compressive strength estimates exceed experimental values, particularly for specimens with multiple geogrid layers. This deviation can be attributed to idealized assumptions in the confinement model that may not fully capture the practical limitations such as geogrid slip, anchorage inefficiencies, and fiber orientation variability. While the analytical approach provides a useful order-of-magnitude estimate, it does not reflect the post-cracking interaction mechanisms and degradation captured in physical testing. Similar trends have been reported by DAOU *et al*. [6] and MANDER *et al*. [17] where theoretical confinement models overpredict strength in cases of imperfect material behavior.

3.2. Impact of geogrid internal confinement on axial load carrying capacity

Figure 9 displays the axial load vs. axial displacement curve of samples with varying numbers of geogrid layers used to provide a confining effect, including UC (unconfined), C-E-1L, C-E-2L, and C-E-3L. First, there is a phase of linearity in the load-displacement behaviour that lasts for about 70% of the ultimate load. After then, a nonlinear stage is reached by the curve, where significant strains start to show up for small increments of loads. Unconfined specimen (UC) fails to exhibit appreciable post-peak behavior. The specimen is crumbled

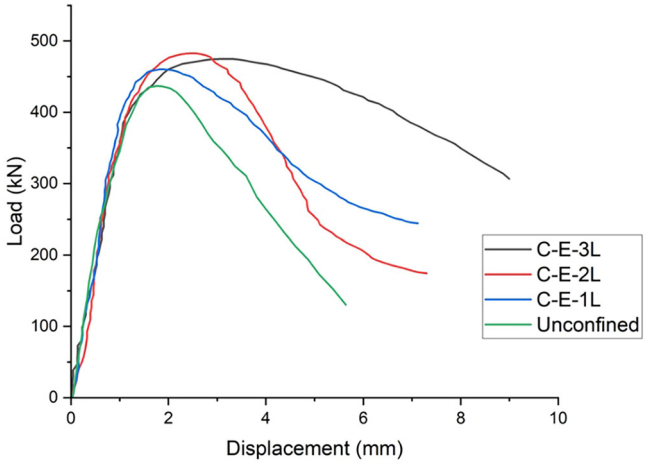

Figure 9: Confinement effect of geogrid.

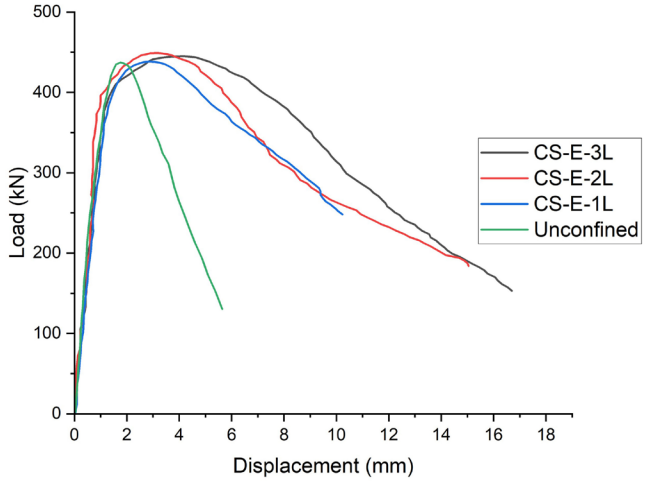

Figure 10: Confinement effect of geogrid and steel fiber.

at the ultimate load. When inner geogrid confinement was not present, concrete sample deterioration occurred before the sample failure. It could be seen in Figure 12b, c, d that specimens C-E-1L, C-E-2L, and C-E-3L fail in a way that causes the volume to expand, which causes a perpendicular fracture. However, there is no concrete crushing or geogrid degradation. The post-peak response given by the specimens with geogrid confinement is noticeably better when compared to unconfined specimens (UC). The sample with one layer of geogrid (C-E-1L) achieved a 5% higher ultimate load than the unconfined control specimen. The sample with a double geogrid layer (C-E-2L) and a triple geogrid layer (C-E-3L), on the other hand, had an ultimate load that was about 10% higher for the double layer and 8% higher for the triple layer than the unconfined control specimen.

Figure 10 displays the axial load vs. axial displacement curve of samples with varying numbers of geogrid layers and steel fiber used to provide a confining effect, including UC (unconfined), CS-E-1L, CS-E-2L, and CS-E-3L. The sample with one layer of geogrid and steel fiber (CS-E-1L) achieved a 0.3% higher ultimate load than the unconfined control specimen. The sample with a double geogrid layer and steel fiber (CS-E-2L) and a triple layer geogrid and steel fiber (CS-E-3L), on the other hand, had an ultimate load that was about 2.7% higher for the double layer with steel fiber and 1.8% higher for the triple layer geogrid and steel fiber than the unconfined control specimen.

Figure 11 displays the axial load vs. axial displacement curve of samples with varying numbers of geogrid layers and PVA fiber used to provide a confining effect, including UC (unconfined), CP-E-1L, CP-E-2L, and

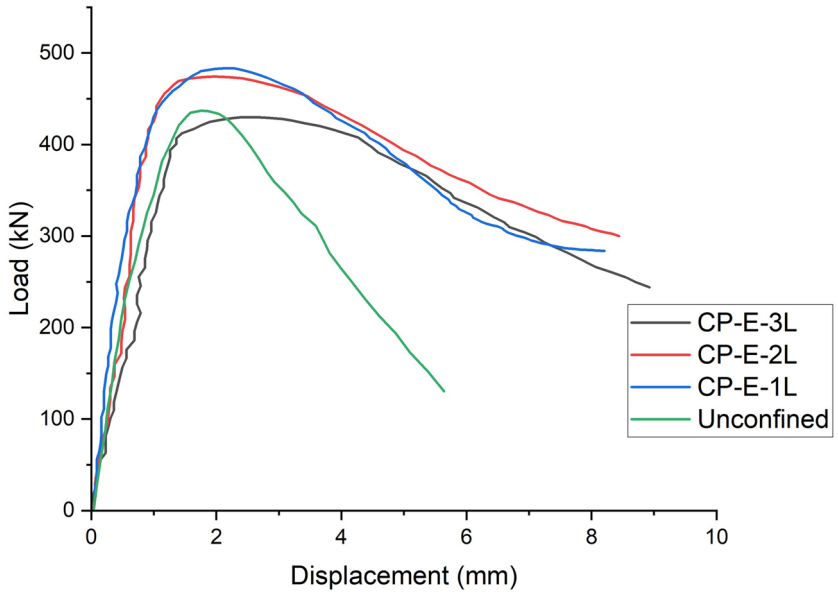

Figure 11: Confinement effect of geogrid and PVA fiber.

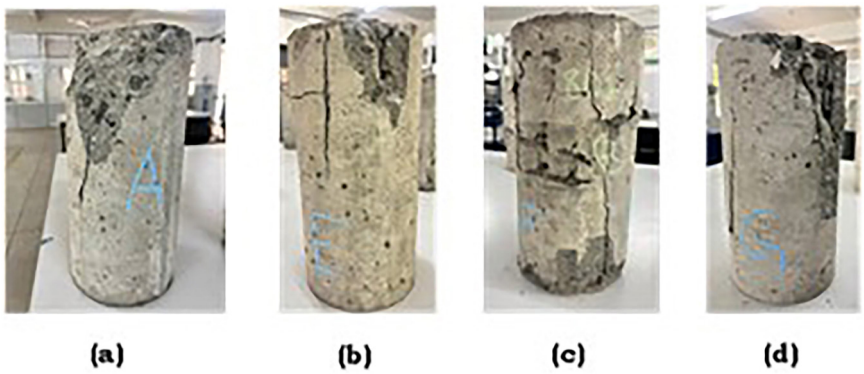

Figure 12: Failure of samples: (a) C, (b) C-E-1L, (c) C-E-2L, (d) C-E-3L.

CP-E-3L. The sample with one layer of geogrid and PVA fiber (CP-E-1L) achieved a 10.6% higher ultimate load than the unconfined control specimen. The sample with a double geogrid layer and PVA fiber (CS-E-2L) and a triple layer geogrid and PVA fiber (CS-E-3L), on the other hand, had an ultimate load that was about 8.5% higher for the double layer with steel fiber and 1.6% lower for the triple layer geogrid and PVA fiber than the unconfined control specimen.

3.3. Combined impact of steel fibre and geogrid confinement on displacement

The load deformation behavior of the samples having steel fiber and geogrid confinement is remarkably enhanced when compared with the unconfined specimen. Figure 10 illustrates the behavior clearly. Figure 12 and Figure 13 illustrates the pattern of failure. The experienced ultimate displacement value of the sample with one layer of geogrid and steel fiber (CS-E-1L) is 10.23 mm, which is 2.258 times greater than unconfined sample C. Similarly, the ultimate displacement experienced by the sample with a double geogrid layer and steel fiber (CS-E-2L) and a triple layer geogrid and steel fiber (CS-E-3L) was about 2.778 times and 2.783 times higher than the unconfined control specimen. Specimen with steel fiber and geogrid has a more ductile failure pattern in comparison to other samples, as seen by its post-peak behavior.

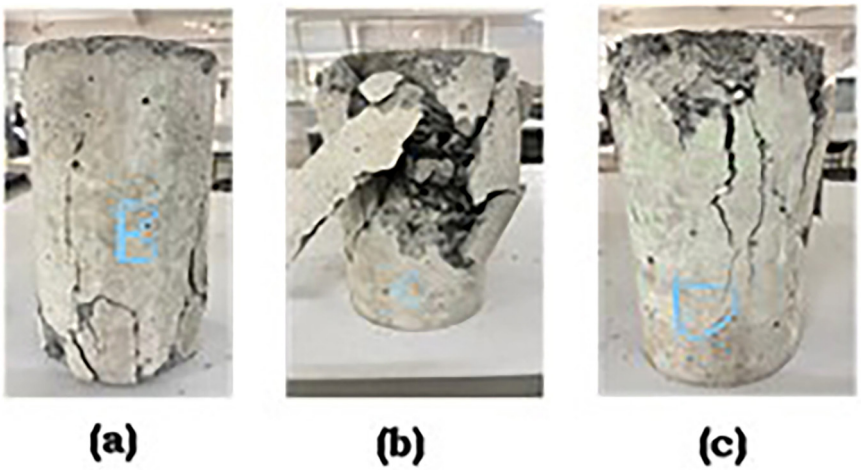

Figure 13: Failure of samples: (a) CS-E-1L, (b) CS-E-2L, (c) CS-E-3L.

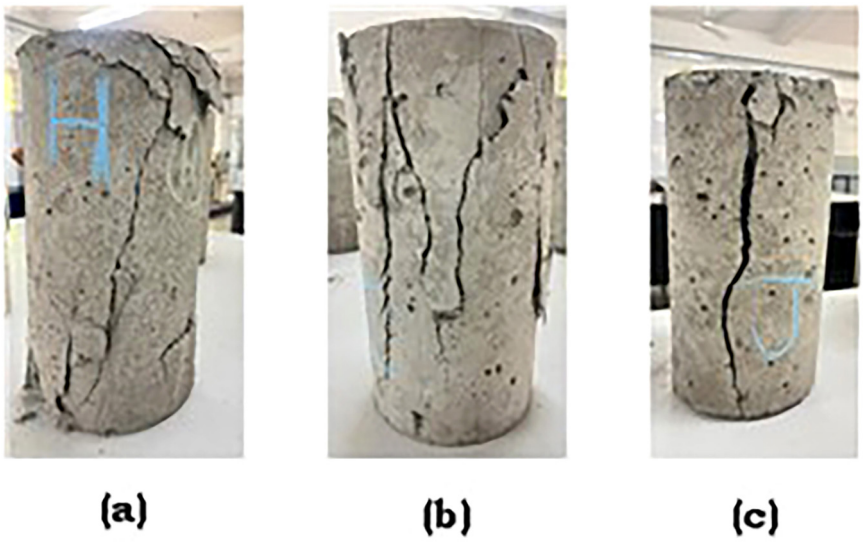

Figure 14: Failure of samples: (a) CP-E-1L, (b) CP-E-2L, (c) CP-E-3L.

3.4. Combined impact of PVA fibre and geogrid confinement on displacement

The load deformation behavior of the samples having PVA fiber and geogrid confinement is considerably enhanced when compared with the unconfined specimen. Figure 11 illustrates the behavior clearly. Figure 14 illustrates the pattern of failure. The experienced ultimate displacement value of the sample with one layer of geogrid and PVA fiber (CP-E-1L) is 8.21 mm, which is 1.812 times greater than unconfined sample C. Similarly, the ultimate displacement experienced by the sample with a double geogrid layer and PVA fiber (CP-E-2L) and a triple layer geogrid and PVA fiber (CP-E-3L) was about 1.863 times and 1.971 times, respectively, greater than the unconfined control sample. Sample with PVA fiber and geogrid has a more ductile failure pattern in comparison to other samples, as seen by its post-peak behavior. When looking at the deflection values, the samples with PVA fiber and geogrid (CP-E-1L, CP-E-2L, CP-E-3L) showed less deflection compared to the samples with steel fiber and geogrid (CS-E-1L, CS-E-2L, CS-E-3L). From Figure 15, it is evident that samples confined with a 3-layer geogrid and steel fibers dissipate greater energy and are also subjected to larger displacement.

3.5. Impact of confinement on the index for displacement ductility (μ)

The deviation in index for displacement ductility (μ) is shown in Figure 16. The index for displacement ductility (μ) value indicates that the deformation capacity for the specimens having geogrid confinement is comparatively

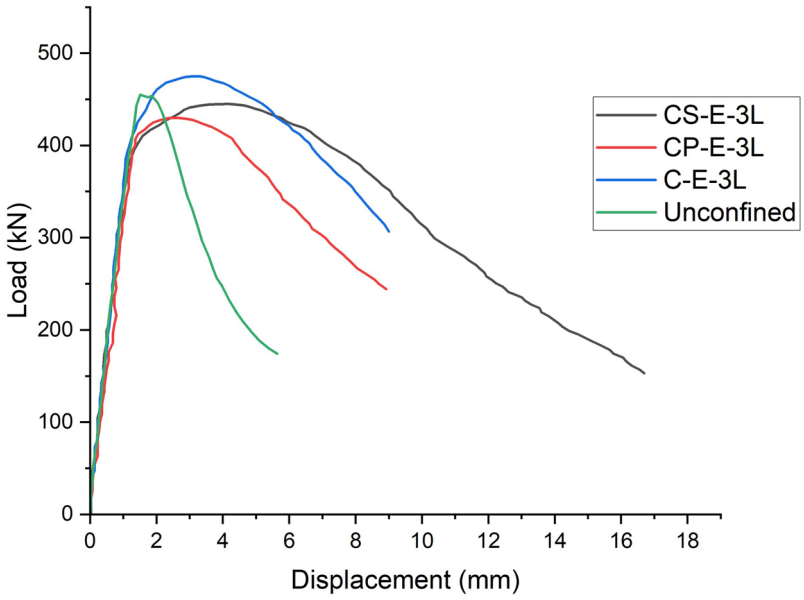

Figure 15: Load-displacement curves for three-layer geogrid confined samples.

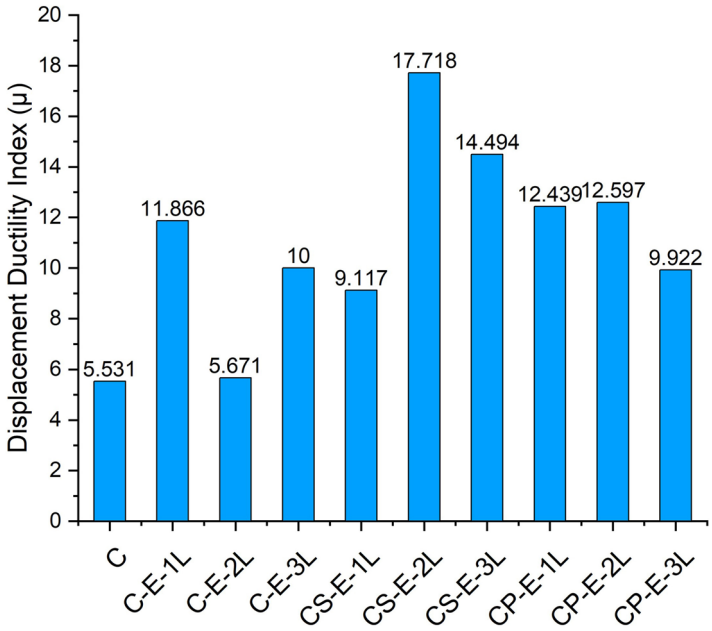

Figure 16: Deviation in index for displacement ductility (μ) defined using the axial deformation ratios (δ_f to δ_y).

higher than that of the concrete specimens without any geogrid. The displacement ductility index value (μ) for the sample with one layer of geogrid (C-E-1L) was 11.867, which is about twice as high as the value for the control sample (C) that did not have any geogrid confinement. On the other hand, the displacement ductility index value (μ) for the sample with a double geogrid layer (C-E-2L) is only 2.5% higher than the control sample (C). Whereas the sample with a triple geogrid layer (C-E-3L) had a displacement ductility value (μ) of 10 that was about 80% higher than the unconfined control specimen.

The CS-E-1L sample has a displacement ductility index value (μ) of 9.188, which is about 60% higher than the control sample (C). This is because it has one layer of geogrid and steel fiber. Also, the μ value for the sample with two layers of geogrid and steel fiber (CS-E-2L) and three layers of geogrid and steel fiber (CS-E-3L)

was 17.718 and 14.494, respectively. This is about three times higher than the value for the control sample (C). Also, the samples that were confined with geogrid and PVA fibers had a higher μ value than the samples that were not confined and the samples that were confined with geogrid alone. The sample with one layer of geogrid and PVA fiber (CP-E-1L) has a μ value of 12.43, which is about twice as high as the value for the control sample (C). The μ value for the sample with two layers of geogrid and PVA fiber (CP-E-2L) and three layers of geogrid and PVA fiber (CP-E-3L) was also 12.297 and 9.922, which is higher than the value for the control sample (C).

3.6. Impact of confinement on the index for energy ductility

The deviation in index for energy ductility (K) is shown in Figure 17. The index for energy ductility (K) value is one more intimation of the beneficial impact of confinement provided by geogrid related to the absorption of energy. The samples confined with geogrids showed higher energy absorption. It has an energy ductility index value of 1.682 for the sample with one layer of geogrid (C-E-1L), 1.608 for the sample with two layers of geogrid (C-E-2L), and 2.518 for the sample with three layers of geogrid (C-E-3L). The samples incorporated with steel fibers and confined with geogrid had a higher K value than the unconfined sample and the samples confined with geogrid alone. The energy ductility index value (K) of the sample with one layer of geogrid and steel fiber (CS-E-1L) is 2.488. Similarly, the sample with a double geogrid layer and steel fiber (CS-E-2L) and a triple-layer geogrid and steel fiber (CS-E-3L) displayed a K value of 2.99 and 3.22, respectively. Also, the samples incorporated with PVA fibers and confined with geogrid had a higher K value than the unconfined sample and the samples confined with geogrid alone. The energy ductility index value (K) of the sample with one layer of geogrid and PVA fiber (CP-E-1L) is 2.161. Similarly, the sample with a double geogrid layer and PVA fiber (CP-E-2L) and a triple-layer geogrid and PVA fiber (CP-E-3L) displayed a K value of 2.252 and 2.12, respectively.

3.7. Comparison with existing studies

The outcomes of this investigation were compared with previously published research to assess the effectiveness of geogrid confinement and fiber reinforcement in enhancing the structural behavior of concrete elements.

AL-AYASH *et al*. [7] demonstrated that confinement with uniaxial and biaxial geogrids in plain concrete cylinders improved ductility and post-cracking behavior. Similar improvements were observed in this study, where the displacement ductility index (μ) for specimens with geogrid confinement reached up to 11.867, which is significantly higher than the control sample (μ = 5.531). The use of PVA and steel fibers further enhanced ductility, showing consistency with the observations by SIVA CHIDAMBARAM and AGARWAL [12].

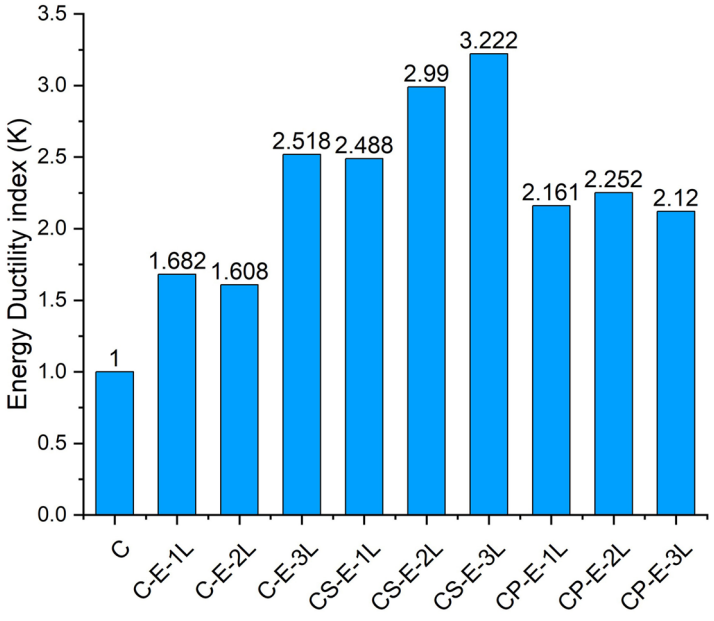

Figure 17: Deviation in index for energy ductility (K) defined using the fracture energy ratio.

EL MESKI and CHEHAB [8] reported that beams reinforced with geogrids exhibited higher deflection and ductile failure modes compared to unreinforced concrete. This aligns with the results of this study, where stub columns with geogrid and fiber reinforcement displayed improved post-peak behavior and energy absorption. The energy ductility index (K) reached values as high as 3.22 for CS-E-3L, demonstrating enhanced fracture energy absorption similar to findings by EL MESKI and CHEHAB [8].

SIVA CHIDAMBARAM and AGARWAL [12, 14] found that geogrid and steel fiber combinations significantly enhanced the load-displacement behavior and energy dissipation in reinforced concrete beams. The current study corroborates this result by showing that the combined action of steel fibers and geogrid (CS-E series) substantially increased both the ductility index and energy ductility index compared to geogrid-only specimens. For instance, CS-E-3L showed a K value of 3.222 compared to 2.518 for C-E-3L (geogrid only), confirming the synergistic effect.

Moreover, TANG *et al*. [9] highlighted that increasing the number of geogrid layers improved post-cracking ductility and energy absorption in concrete members. This is supported by the present results, where increasing from one to three layers of geogrid improved both μ and K indices, although the ultimate load did not increase proportionally.

These comparisons suggest that the present findings are consistent with and extend previous research by focusing on stub column behavior under axial compression. They further validate geogrid confinement, especially in combination with fiber reinforcement, as an effective method to enhance ductility and energy absorption in structural concrete elements.

3.8. Comparison with international design codes

The observed enhancements in axial load capacity and ductility of geogrid-confined concrete stub columns can be contextually aligned with existing international design recommendations, particularly those found in the CEB-FIP Model Code 1990 and ACI 440.2R-17.

The CEB-FIP Model Code 1990 [35] introduces a confinement model that relates the increase in concrete strength and strain capacity to the lateral confining pressure provided by transverse reinforcement. Although this code is primarily formulated for steel or FRP confinement, the principle of increased strain capacity due to lateral restraint is directly applicable to the geogrid-confined specimens tested in this study. The improved displacement ductility indices (up to 17.7 for CS-E-2L) and energy ductility indices (up to 3.22 for CS-E-3L) observed in this study are consistent with the expected behavior of confined concrete as per the CEB-FIP model.

Similarly, ACI 440.2R-17 [36] provides guidance for the confinement of concrete using externally bonded fiber-reinforced polymers (FRPs). It introduces confinement efficiency factors to predict the ultimate strength and strain of confined concrete. While ACI 440 is tailored for FRP wraps, the experimental outcomes in this study suggest that internal geogrid confinement exhibits comparable post-peak ductile behavior and moderate strength enhancement. Specifically, the use of PVA fibers with geogrid (e.g., CP-E-1L and CP-E-2L) achieved up to 10.6% strength improvement, in alignment with ACI's documented strength gains for moderate confinement levels.

3.9. Theoretical considerations and future work

The experimental results of this study demonstrate that geogrid confinement, especially when combined with steel or PVA fibers, significantly enhances the ductility and energy absorption capacity of concrete stub columns. To further understand and predict these enhancements, the principles outlined in the CEB-FIP Model Code 90 [35] can be utilized. This code provides comprehensive guidelines for quantifying the confinement-induced enhancement of concrete strength and ductility, primarily through the application of lateral confining pressures.

While the CEB-FIP Model Code 90 primarily addresses confinement effects due to transverse steel reinforcement, its concepts can be extended to alternative confinement materials such as geogrids. Incorporating these principles into finite element modeling (FEM) could offer predictive insights into the structural behavior of geogrid-confined concrete elements. Notably, the work by AL-AYASH *et al*. [37] demonstrates how hardening effects were incorporated into FEM analysis using confinement principles. Adopting such an approach in future numerical modeling of geogrid-confined stub columns could bridge the gap between experimental results and structural design guidelines.

3.10. Practical implications

The outcomes of this study have significant practical applications in the construction industry, particularly for structures requiring improved ductility and moderate load enhancement without increasing conventional reinforcement. The use of uniaxial geogrids as internal confinement offers a corrosion-resistant, cost-effective, and

lightweight alternative to traditional steel stirrups in stub columns. This is especially beneficial for pre-cast or modular construction where ease of fabrication and durability are critical. Additionally, the combination of geogrids with steel or PVA fibers can be employed in seismic zones or infrastructure subjected to dynamic or impact loads, where enhanced energy dissipation and crack control are essential. These findings pave the way for incorporating geogrid-confined concrete columns into design practices aimed at improving the resilience and service life of structural elements.

4. CONCLUSION

The study used twenty small-scale stub column samples to assess the impact of confinement provided by geogrid on the ultimate axial load and the axial load-axial deformation relationship. The experimental test's results could lead to the following conclusions.

- Geogrid confinement improved the axial load capacity of stub columns, with double and triple layers increasing the load by 10% and 8%, respectively.
- The samples with steel fibers and geogrid confinement had higher fracture energies than the samples with PVA fibers and geogrid confinement. Particularly, samples with three geogrid layers exhibited higher fracture energies.
- According to the results of the compression test on geogrid-reinforced concrete samples, the structural integrity linked to the geogrid plus fibers, especially steel fibers, can significantly improve the load-deformation behaviors along with crack development.
- Geogrid and fiber reinforcement significantly improved load-deformation behavior, ductility, and fracture energy.
- While geogrid confinement had a limited impact on ultimate load capacity, it greatly enhanced the ductility and energy absorption of concrete specimens.
- Geogrid provides a promising, corrosion-resistant, and lightweight alternative to conventional confinement methods.

To compare the confinement impact of uniaxial geogrid sheets to biaxial geogrids, additional studies must be done. Also, it would be important to compare the effects of aggressive environments on concrete stub columns confined with geogrids.

5. BIBLIOGRAPHY

[1] XIONG, C.N., SHAO, Y.B., TONG, L.W., *et al*., "Static strength of CFRP-strengthened preloaded circular concrete-filled steel tube stub column columns – part II": theoretical and numerical analysis", *Thin-walled Structures*, v. 184, pp. 110547, 2023. doi: http://doi.org/10.1016/j.tws.2023.110547.

[2] HUANG, Y., LIANG, H., LU, Y., *et al*., "Axial behaviour of square stub CFST columns strengthened with square steel tube and HPC jacket", *Journal of Constructional Steel Research*, v. 186, pp. 106896, 2021. doi: http://doi.org/10.1016/j.jcsr.2021.106896.

[3] ABDESSSEMED, M., KENAI, S., BALI, A., "Experimental and numerical analysis of the behavior of an airport pavement reinforced by geogrids", *Construction & Building Materials*, v. 94, pp. 547–554, 2015. doi: http://doi.org/10.1016/j.conbuildmat.2015.07.037.

[4] KHODAII, A., FALLAH, S., MOGHADAS NEJAD, F., "Effects of geosynthetics on reduction of reflection cracking in asphalt overlays", *Geotextiles and Geomembranes*, v. 27, n. 1, pp. 1–8, 2009. doi: http://doi.org/10.1016/j.geotexmem.2008.05.007.

[5] MAXWELL, S., KIM, W.H., EDIL, T.B., *et al*., *Effectiveness of geosynthetics in stabilizing soft subgrades final report*, Wisconsin, EUA: Wisconsin Department of Transportation, 2006.

[6] DAOU, A., CHEHAB, G., SAAD, G., *et al*., "Experimental and numerical investigations of reinforced concrete columns confined internally with biaxial geogrids", *Construction & Building Materials*, v. 263, pp. 120115, 2020. doi: http://doi.org/10.1016/j.conbuildmat.2020.120115.

[7] AL-AYASH, Z., KAHIL, S.N., KARAKASHIAN, A., *et al*., "Application of existing numerical models for prediction of geogrid confinement effectiveness of PCC columns", In: *Proceedings of the Geosynthetics Conference*, Portland, Oregon, 2015.

[8] EL MESKI, F., CHEHAB, G.R., "Flexural behavior of concrete beams reinforced with different types of geogrids", *Journal of Materials in Civil Engineering*, v. 26, n. 8, pp. 04014038, 2014. doi: http://doi.org/10.1061/(ASCE)MT.1943-5533.0000920.

[9] TANG, X., HIGGINS, I., JLILATI, M.N., "Behavior of geogrid-reinforced Portland cement concrete under static flexural loading", *Infrastructures*, . 3, n. 4, pp. 41, Sep. 2018. doi: http://doi.org/10.3390/infrastructures3040041.

[10] SIVAKAMASUNDARI, S., DANIEL, A.J., KUMAR, A., "Study on flexural behavior of steel fiber rc beams confined with biaxial geo-grid", *Procedia Engineering*, v. 173, pp. 1431–1438, 2017. doi: http://doi.org/10.1016/j.proeng.2016.12.206.

[11] AL-HEDAD, A.S.A., BAMBRIDGE, E., HADI, M.N.S., *et al*., "Influence of geogrid on the drying shrinkage performance of concrete", *Construction & Building Materials*, v. 146, pp. 165–174, 2017. doi: http://doi.org/10.1016/j.conbuildmat.2017.04.076.

[12] SIVA CHIDAMBARAM, R., AGARWAL, P., "The confining effect of geo-grid on the mechanical properties of concrete specimens with steel fiber under compression and flexure", *Construction & Building Materials*, v. 71, pp. 628–637, 2014. doi: http://doi.org/10.1016/j.conbuildmat.2014.08.059.

[13] SIVA CHIDAMBARAM, R., AGARWAL, P., "Performance evaluation of geogrid-confined beam-column joints with steel fiber reinforced concrete under cyclic loading", *Journal of Testing and Evaluation*, v. 44, n. 1, pp. 582–598, 2016. doi: http://doi.org/10.1520/JTE20150037.

[14] SIVA CHIDAMBARAM, R., AGARWAL, P., "Flexural and shear behavior of geo-grid confined RC beams with steel fiber reinforced concrete", *Construction & Building Materials*, v. 78, pp. 271–280, 2015. doi: http://doi.org/10.1016/j.conbuildmat.2015.01.021.

[15] SIVA CHIDAMBARAM, R., AGARWAL, P., "Shear resistance behaviour of geogrid-confined RC elements under static and cyclic loading", *Current Science*, v. 117, n. 2, pp. 260–271, 2019. doi: http://doi.org/10.18520/cs/v117/i2/260-271.

[16] YALCINER, H., KUMBASAROGLU, A., ERTUC, İ., *et al*., "Confinement effect of geo-grid and conventional shear reinforcement bars subjected to corrosion", *Structures*, v. 13, pp. 139–152, 2017. doi: http://doi.org/10.1016/j.istruc.2017.12.004.

[17] MANDER, J.B., PRIESTLEY, M.J.N., PARK, R., "Theoretical stress-strain model for confined concrete", *Journal of Structural Engineering*, v. 114, n. 8, pp. 1804–1826, 1988. doi: http://doi.org/10.1061/(ASCE)0733-9445(1988)114:8(1804).

[18] HADI, M.N.S., "Behaviour of FRP wrapped normal strength concrete columns under eccentric loading", *Composite Structures*, v. 72, n. 4, pp. 503–511, 2006. doi: http://doi.org/10.1016/j.compstruct.2005.01.018.

[19] LAM, L., TENG, J.G., "Design-oriented stress-strain model for FRP-confined concrete", *Construction & Building Materials*, v. 17, n. 6-7, pp. 471–489, 2003. doi: http://doi.org/10.1016/S0950-0618(03)00045-X.

[20] LI, J., HADI, M.N.S., "Behaviour of externally confined high-strength concrete columns under eccentric loading", *Composite Structures*, v. 62, n. 2, pp. 145–153, 2003. doi: http://doi.org/10.1016/S0263-8223(03)00109-0.

[21] FAM, A., RIZKALLA, S.H., "Behavior of axially loaded concrete-filled circular fiber-reinforced polymer tubes", *ACI Structural Journal*, v. 98, pp. 280–289, 2001.

[22] VELAYUTHAM, S., LEE, Y.H., HE, S., "Structural performance of GFRP-concrete-steel composite columns subjected to eccentric axial loading", *Advances in Structural Engineering*, v. 27, n. 4, pp. 623–637, 2024.

[23] SALMAN, B.F., ALLAWI, A.A., "Experimental and numerical investigation on the behavior of composite reinforced concrete columns encased by steel section and hybrid GFRP section", *Advances in Structural Engineering*, 2025. In press. doi: http://doi.org/10.1177/13694332251322587.

[24] AHMED, H.S., ALLAWI, A., HINDI, R., "Experimental investigation of composite circular encased GFRP I-section concrete columns under different load conditions", *Engineering, Technology & Applied Science Research*, v. 14, n. 5, pp. 17286–17293, 2024. doi: http://doi.org/10.48084/etasr.8521.

[25] ALLAWI, A., AHMED, H.S., HINDI, R., "A numerical study of concrete composite circular columns encased with gfrp i-section using the finite element method", *Engineering, Technology & Applied Science Research*, v. 15, n. 1, pp. 19478–19483, 2025. doi: http://doi.org/10.48084/etasr.9332.

[26] SALMAN, B.F., ALLAWI, A.A., "Strength and deformation of encased concrete columns by I-section steel and I-section GFRP subjected to different load conditions", *Heliyon*, v. 10, n. 23, e40504, 2024. doi: http://doi.org/10.1016/j.heliyon.2024.e40504. PubMed PMID: 39660182.

[27] RAVIKUMAR, K., PALANICHAMY, S., SINGARAM, C.J., *et al*., "Crushing performance of pultruded GFRP angle section with various connections and joints on lattice towers", *Matéria*, v. 29, n. 1, e20230003, 2023. doi: http://doi.org/10.1590/1517-7076-RMAT-2023-0003.

[28] ASSUNÇÃO, I.M., SILVA, L.D., BASTOS, J.F., *et al*., "Mechanical properties of glassfiber reinforced polyester composites manufactured by two different sprayup techniques", *Matéria*, v. 29, e20240450, 2024. doi: http://doi.org/10.1590/1517-7076-rmat-2024-0450.

[29] SHAHRBIJARI, K.B., BARROS, J.A., VALENTE, I.B., "Study on the structural performance of concrete beams reinforced with pre-stressed GFRP and steel bars", *Revista de la Construcción*, v. 22, n. 2, pp. 262–273, 2023. doi: http://doi.org/10.7764/RDLC.22.2.262.

[30] BUREAU OF INDIAN STANDARDS, *IS 10262:2019 concrete mix proportioning – guidelines*, 2 ed., New Delhi, BIS, 2019.

[31] BUREAU OF INDIAN STANDARDS, *IS 456:2000 plain and reinforced concrete – code of practice*, New Delhi, BIS, 2000.

[32] AMERICAN CONCRETE INSTITUTE, *ACI 318-19 building code requirements for structural concrete*, Farmington Hills, MI, ACI Committee, 2022.

[33] AMERICAN SOCIETY FOR TESTING AND MATERIALS, *ASTM D6637-11 standard test method for determining tensile properties of geogrids by the single or multi-rib tensile method*, West Conshohocken, ASTM, 2011.

[34] EUROPEAN UNION, *EN 1992-1-1 Eurocode 2: design of concrete structures—part 1-1: general rules and rules for buildings*, Geneva, 2004.

[35] COMITÉ EURO-INTERNATIONAL DU BÉTON, *CEB-FIP Model Code 1990: design code*, London, CEB, 1993.

[36] AMERICAN CONCRETE INSTITUTE, *ACI 440.2R-17 guide for the design and construction of externally bonded FRP systems for strengthening concrete structures*, Farmington Hills, MI, 2017.

[37] AL-AYASH, A., AL-MAHAIDI, R., AL-MAHMOUD, F., "Numerical simulation of the confinement effect in FRP-confined concrete cylinders using a modified stress–strain model", *Structural Engineering and Mechanics*, v. 61, n. 3, pp. 365–377, 2017.